

# Optimizing Multi-grid Based Reduction for Efficient Scientific Data Management

Xin Liang, Ben Whitney, Jieyang Chen, Lipeng Wan, Qing Liu, Dingwen Tao,  
James Kress, Dave Pugmire, Matthew Wolf, Norbert Podhorszki, and Scott Klasky

**Abstract**—Data management becomes increasingly important in dealing with the large amounts of data produced by today's large-scale scientific simulations and experimental instrumentation. Multi-grid compression algorithms provide a promising way to manage scientific data at scale, but are not tailored for performance and reduction quality. In this paper, we optimize a multi-grid based algorithm to achieve high-performance and high-quality error-controlled lossy compression. Our contributions are three-fold. 1) We quantize the multi-grid coefficients in a level-wise fashion, and leverage multi-grid decomposition as a preconditioner instead of standalone compressors to improve compression ratios. 2) We optimize the performance of multi-grid decomposition/recomposition with a series of techniques from both system-level and algorithm-level. 3) We evaluate our proposed method using four real-world scientific datasets and compare with several state-of-the-art lossy compressors. Experiments demonstrate that our optimizations improve the decomposition/recomposition performance of the existing multi-grid based approach by up to  $70\times$ , and the proposed compression method can improve compression ratio by up to  $2\times$  compared with the second best error-controlled lossy compressors under the same distortion.

**Index Terms**—Lossy Compression, Multi-grid Decomposition, Error Control, Scientific Data.

## 1 INTRODUCTION

WITH the extremely large amounts of data produced by large-scale scientific simulations on leadership high-performance computing (HPC) systems and experimental instrumentation, the management of those data has become a serious problem. On the one hand, not all the data can be stored in fast storage device such as parallel file systems. They have to be moved to slow storage devices such as archives, where data transfer time will become prohibitive because of the limited bandwidth. On the other hand, even if the full data could be stored, post hoc analysis on the entire data would be too costly to conduct. For instance, the DCA++ code [1] produces 100 TB of data in a single run, but only a small subset, 100 MB of data is written due to the cost in post hoc data analysis. DCA++ scientist reduce their seven dimensional tensor data down to a two dimensional subset, reducing the data by  $10^6$ . This allows the analysis to be easily done on a laptop, but it often loses valuable information which is not captured in the reduced data set.

Error-controlled lossy compression techniques [2], [3], [4], [5], [6], [7], [8], [9] have been proposed and developed in the last decade to address the storage issue, which feature

in reducing data size while controlling distortion of decompressed data. However, these *data reduction* methods suffer from large distortion when required compression ratio is relatively high (e.g.  $30\times$ ), although such compression ratio is a common demand in HPC community. For example, ZFP [3] exhibits visual artifact when the compression ratio reaches  $64\times$  according to previous studies [7]. SZ [7] generates visually better results thanks to its multi-algorithm design, but the compression ratios it gets under certain distortion are still not satisfactory. The hybrid model proposed in [9] significantly improves the quality by leveraging the orthogonal transform in ZFP as a predictor in SZ along with block-wise adaptive selection, but suffers from high computational overhead. Because of the rapid growth of the data volumes, more efficient methods need to be explored to improve the data reduction quality.

Recently, multigrid-based methods [10], [11], [12] have been proposed by the applied math community to address the data issues by providing an efficient way for scientific data reduction. Specifically, these methods decompose data into a collection of components of progressively finer resolution based on the theories of wavelet analysis, finite element methods, and multigrid linear solvers. These components (also called multi-grid levels) are represented in a basis chosen to allow quasi-optimal implementations of the decomposition and recomposition stages and to facilitate error-bounded compression by quantization of the basis coefficients. These existing works offer an elegant way to deal with scientific data, but suffer from limited performance and compression quality.

Besides data reduction, the multi-grid based data decomposition can also be used for data refactoring, which reduces the complexity of post hoc analysis in addition to data volumes. Unlike data reduction which always reconstructs

- X. Liang, B. Whitney, J. Chen, L. Wan, J. Kress, D. Pugmire, M. Wolf, N. Podhorszki, S. Klasky are with the Computer Science and Mathematics Division, Oak Ridge National Laboratory, Oak Ridge, TN 37830.  
E-mail: {liangx, chenj3, wanl, whitneybe, kressjm, pugmire, wolfdnd, pnorbort, klasky}@ornl.gov
- Q. Liu is with the Helen and John C. Hartmann Department of Electrical and Computer Engineering, New Jersey Institute of Technology, Newark, NJ 07102.  
E-mail: qliu@njit.edu
- D. Tao is with the School of Electrical Engineering & Computer Science, Washington State University, Pullman, WA 99163.  
E-mail: dingwen.tao@wsu.edu

Manuscript received Oct. 11, 2020. (X. Liang and B. Whitney were co-first authors of this work.)

data to the same degrees of freedom as the original data, data refactoring is able to decompose the original data into a series of hierarchical representations with increasing degrees of freedom. Compared with data reduction, data refactoring may incur larger distortion in the reconstructed data, but is able to 1) progressively reconstruct data with increased precision and 2) provide coarse grained representations that can be used to perform post hoc data analysis with greatly reduced complexity.

This work focuses on improving the efficiency of multi-grid based data reduction for both performance and quality. Specifically, we propose two novel techniques to improve the compression ratios for multi-grid based data reduction while maintaining the same distortion. We also apply a series of optimizations to the multigrid methods, which boost the performance for both data decomposition and recombination. In summary, our contributions are as follows:

- We propose two novel techniques to significantly improve the quality of error-controlled multi-grid based data reduction in terms of Peak signal-to-Noise-Ratio (PSNR), which is widely used metric for lossy compression according to literature [2], [3], [7], [9], [13]. In particular, we propose to quantize the multi-grid coefficients with separate error bounds for each level and carefully derive the best-fit relationship for the error bounds across levels. We also propose to decompose data in an adaptive fashion where the decomposition stops at the most appropriate level and leverages external compressors to compress the remaining coarse representation efficiently.
- We implement the proposed method with a series of optimizations to provide high-performance error-bounded lossy compression for scientific data. Specifically, we adopt a level-centric data reorder strategy and batched operations to improve the cache coherence and memory efficiency. We also revise the correction computation kernel (which is one of the most important steps in the multi-grid decomposition/recomposition algorithms) to reduce the computational cost.
- We evaluate our method with respect to both performance and quality using four real-world datasets from different scientific applications. We first demonstrate the effectiveness of the proposed optimizations compared to original multi-grid based approach [11], and then compare our method with state-of-the-art error-bounded lossy compressors including SZ [7], ZFP [3], and the hybrid model [9]. Experimental results show that the proposed framework has  $20 \sim 70\times$  performance improvement compared with the previous multi-grid implementation in terms of decomposition/recomposition speed, and keeps the almost linear speedup with respect to scalability thanks to the embarrassingly parallel nature. In addition, evaluation results on the iso-surface mini-analysis indicate that conducting scientific analysis on coarse-grained representations could significantly improve the analysis performance, while maintaining certain accuracy of the analysis result. Furthermore, the compression ratios of the proposed approach is  $2\times$  improvement compared with that of the best error-controlled lossy compressors

[3], [7], [9] under the same distortion in high compression ratio cases, showing great potential in reducing storage capacity and mitigating I/O bottleneck.

The rest of the paper is organized as follows. In Section 3, we specify the metrics for evaluation. In Section 4, we propose level-wise quantization and multi-grid based preconditioning to improve the quality of error-controlled lossy compression. In Section 5, we introduce the sets of optimization techniques applied to the framework. In Section 6, we evaluate our method using real-world simulation data from scientific applications. Finally, we discuss the related works in Section 7 and conclude our work in Section 8.

## 2 BACKGROUND

In this section, we describe the central decomposition and recombination routines of MGARD, which serves as the starting point for the multi-grid based method in this work. This description focuses on the computational steps involved. For a full mathematical treatment, see [10], [11].

The input is an array (multidimensional in general)  $u$  of floating-point numbers. We interpret  $u$  as the values taken by some function  $u$  on a grid  $\mathcal{N}_L$  having the same dimensions as  $u$ . For example, if  $u$  has shape  $n_1 \times \dots \times n_d$ , then  $\mathcal{N}_L$  might be  $\{(j_1h, \dots, j_dh) : 0 \leq j_i < n_i\}$ . Each element  $x \in \mathcal{N}_L$  is a point in the domain of  $u$ ; the corresponding entry  $u[(j_1, \dots, j_d)]$  of the array is the value  $u(x)$  taken by the function at that point.

We decompose  $u$  using a sequence  $\mathcal{N}_{L-1}, \dots, \mathcal{N}_0$  of subgrids of  $\mathcal{N}_L$ . We require that the sequence be decreasing, i.e., that  $\mathcal{N}_{l+1} \supset \mathcal{N}_l$ . See Fig. 2 for an example. The blue nodes comprise  $\mathcal{N}_l$ , the blue and yellow nodes comprise  $\mathcal{N}_{l+1}$ , and the blue, yellow, and grey nodes comprise  $\mathcal{N}_{l+2}$ . Denote by  $\mathcal{N}_l^*$  the set  $\mathcal{N}_l \setminus \mathcal{N}_{l-1}$ , with  $\mathcal{N}_{-1} = \emptyset$ . We define for  $0 \leq l \leq L$  operators  $Q_l$  and  $\Pi_l$ , each outputting an array of values defined on  $\mathcal{N}_l$ .

$Q_l$  is an  $L^2$  projection operator. It is applied by computing a matrix-vector product and then solving a linear system.  $\Pi_l$  is a multilinear interpolation operator. It leaves values on  $\mathcal{N}_{l-1}$  unchanged; values on  $\mathcal{N}_l^*$  are determined by interpolating values on  $\mathcal{N}_{l-1}$ .

Mathematically, we can interpret the arrays output by these operators as functions in appropriately defined function spaces. See [10], [11] for details.

The decomposition routine transforms the input function  $u$  to the *multilevel components*  $\{(I - \Pi_{l-1})Q_l u : 0 \leq l \leq L\}$ . This is accomplished by the following iterative procedure, with  $l = L$  for the first iteration.

- 1) Start with  $Q_l u$ , with  $Q_L u = u$ .
- 2) Compute the interpolant  $\Pi_{l-1}Q_l u$ .
- 3) Subtract the interpolant  $\Pi_{l-1}Q_l u$  from  $Q_l u$ , obtaining the multilevel component  $(I - \Pi_{l-1})Q_l u$ .
- 4) Compute the projection  $Q_{l-1}(I - \Pi_{l-1})Q_l u$  of the multilevel component. It can be shown that this projection, which we call the *correction*, is equal to  $Q_{l-1}u - \Pi_{l-1}Q_l u$ .
- 5) Add the correction  $Q_{l-1}u - \Pi_{l-1}Q_l u$  to the interpolant  $\Pi_{l-1}Q_l u$ , obtaining  $Q_{l-1}u$ .
- 6) If  $l = 0$ , stop. Otherwise, decrement  $l$  and repeat.

We call Step 4 the *correction computation* and Step 5 the *correction application*. Steps 2 and 3 are combined in the

implementation into a single operation we call the *coefficient computation*. The coefficients in question are the nodal values  $\{(I - \Pi_{l-1})Q_l u(x) : x \in \mathcal{N}_l^*\}$ . The output of the decomposition routine is an array containing these coefficients for each level  $l$ . When compressing, this array is then quantized; see Subsection 4.1.

The recomposition procedure is the inverse of the decomposition procedure. We start with multilevel components  $\{(I - \Pi_{l-1})Q_l u : 0 \leq l \leq L\}$ . We recover  $u$  by the following iterative procedure, with  $l = 0$  for the first iteration.

- 1) Start with  $Q_{l-1}u$ , with  $Q_{-1}u = 0$ .
- 2) Compute the projection  $Q_{l-1}(I - \Pi_{l-1})Q_l u$  of the multilevel component. As in the decomposition routine, we call this projection the *correction*. It is again equal to  $Q_{l-1}u - \Pi_{l-1}Q_l u$ .
- 3) Subtract the correction  $Q_{l-1}u - \Pi_{l-1}Q_l u$  from  $Q_{l-1}u$ , obtaining the interpolant  $\Pi_{l-1}Q_l u$ .
- 4) Add the interpolant  $\Pi_{l-1}Q_l u$  to the multilevel component  $(I - \Pi_{l-1})Q_l u$ , obtaining  $Q_l u$ .
- 5) If  $l = L$ , stop. Otherwise, increment  $l$  and repeat.

Observe that recomposition involves many of the same subroutines as decomposition. The correction is computed in Step 2 and applied in Step 3, though here it is subtracted, rather than added. Step 4 is the inverse of the coefficient computation.

### 3 METRICS

In this paper, we focus on improving the performance and quality of data refactoring and data reduction using multigrid-based methods. Specifically, we briefly introduce our metrics towards the two objectives in this section.

#### 3.1 Performance

We measure the performance of both multi-grid based decomposition and compression in terms of throughput, which is evaluated by  $\text{size}/t$ , where  $\text{size}$  is the original data size and  $t$  is the time used for the operation. Specifically,  $t$  corresponds to the time for decomposition/recomposition and the time for compression/decompression. The overall performance on a dataset (which may contain multiple fields) is computed by the total size divided by the total time used for the operation.

#### 3.2 Quality

We measure the quality of data reduction using rate-distortion graph [14] which gives an analytical expression for how much compression can be achieved using lossy compression methods. The rate on the  $X$  axis of the graph stands for the average number of bits per data point in the reduced representation, which is the reciprocal of compression ratio multiplied by the number of bits used for original data point. As mentioned before, we adopt PSNR as the distortion metric on the  $Y$  axis of the graph because it indicates overall statistical errors that could be more important than the error bound, especially for visualization purposes. Such metric is consistent with lots of previous works including [2], [3], [7], [9], [13]. Denoting  $\{d_1, d_2, \dots, d_N\}$  and

$\{d'_1, d'_2, \dots, d'_N\}$  as the series of original data and decompressed data where  $N$  is the number data points, PSNR is computed as follows:

$$\text{PSNR} = 20 \log_{10}(\max(d_i) - \min(d_i)) - 10 \log_{10}(\sum_{i=1}^N (d_i - d'_i)^2 / N).$$

According to the definition, higher PSNR indicates less error thus higher quality. Thus, our target on improving data reduction quality turns out to be maximizing the PSNR of decompressed data given the same compression ratio, or equivalently, maximizing the compression ratios given the same PSNR.

## 4 ENHANCED MULTI-GRID BASED REDUCTION

We propose two novel techniques to improve the quality of multi-grid based data reduction with strict error control. In particular, the level-wise quantization strategy significantly improve the compression ratios when error bounds are loose while the adaptive decomposition strategy allows for automatic switch of compression methods in an appropriate level, which leads to comparable performance to existing compressor when error bounds are tight.

### 4.1 Level-wise quantization

MGARD's decomposition routine, described in Section 2, outputs a set of multilevel components  $\{(I - \Pi_{l-1})Q_l u : 0 \leq l \leq L\}$ . Each component is specified by the nodal values  $\{(I - \Pi_{l-1})Q_l u(x) : x \in \mathcal{N}_l^*\}$ . We call these values the *multilevel coefficients* and denote the collection  $u_{\text{mc}}$ .  $u_{\text{mc}}$  is indexed by the nodes of the finest grid  $\mathcal{N}_L$ : given  $x \in \mathcal{N}_L$ , if  $l$  is the least grid index such that  $x \in \mathcal{N}_l$ , then  $u_{\text{mc}}[x] = (I - \Pi_{l-1})Q_l u(x)$ . Following decomposition, the next step in MGARD is to quantize the multilevel coefficients. The output, denoted  $\tilde{u}_{\text{mc}}$ , is then compressed by a lossless encoder.

Just as  $u_{\text{mc}}$  encodes the input function  $u$ ,  $\tilde{u}_{\text{mc}}$  encodes an approximation to  $u$ ,  $\tilde{u}$ . Care must be taken when quantizing that the error  $\|u - \tilde{u}\|_{L^\infty}$  between the two is not greater than the error tolerance  $\tau$  prescribed by the user. It is therefore useful to relate the individual quantization errors  $u_{\text{mc}}[x] - \tilde{u}_{\text{mc}}[x]$  to the overall approximation error  $u - \tilde{u}$ . Such a relationship is given in [10], where it is proved that, for  $C$  a constant depending on the grid hierarchy,

$$\text{if } \sum_{l=0}^L \max_{x \in \mathcal{N}_l^*} |u_{\text{mc}}[x] - \tilde{u}_{\text{mc}}[x]| \leq \frac{\tau}{C}, \quad (1)$$

then  $\|u - \tilde{u}\|_{L^\infty} \leq \tau$ .

In view of this condition, the quantizer has an error 'budget' of  $\tau/C$  to be distributed among the  $L+1$  levels  $\{u_{\text{mc}}[x] : x \in \mathcal{N}_l^*\}$ . Perhaps the simplest strategy, which we call *uniform quantization*, is to split the error budget evenly, quantizing so that  $\max_{x \in \mathcal{N}_l^*} |u_{\text{mc}}[x] - \tilde{u}_{\text{mc}}[x]| \leq (\tau/C)/(L+1)$  for all  $0 \leq l \leq L$ . This is the technique used in the current implementation of MGARD [15].

The next task is to quantize each  $u_{\text{mc}}[x]$  so that  $|u_{\text{mc}}[x] - \tilde{u}_{\text{mc}}[x]| \leq (\tau/C)/(L+1)$ . This can be accomplished by splitting the range of the multilevel coefficients into labelled bins of uniform width  $q$ . Each coefficient  $u_{\text{mc}}[x]$  can then be mapped to the label of the

bin containing it. That label encodes  $\tilde{u}_{\text{mc}}[x]$ . If we choose  $\tilde{u}_{\text{mc}}[x]$  to be the center of the bin, then  $|u_{\text{mc}}[x] - \tilde{u}_{\text{mc}}[x]| \leq q/2$ , since the bin has width  $q$  and contains  $u_{\text{mc}}[x]$ . If the range of the multilevel coefficients has size  $R = \max(u_{\text{mc}}) - \min(u_{\text{mc}})$ , then  $\lceil R/q \rceil$  labels suffice to quantize all of the multilevel coefficients with error at most  $q/2$ . With uniform quantization, the maximum allowed error is  $(\tau/C)/(L+1)$ , so we take  $q$  to be  $(2\tau/C)/(L+1)$ . After quantization, the labels are passed to a lossless encoder for compression.

How many bits are required to store the labels produced by uniform quantization? The exact answer will depend on the distribution of the multilevel coefficients and the lossless encoder used, but we can estimate the cost using Shannon entropy [16]. Informally and in brief, the cost in bits per symbol to encode a stream is bounded below by the Shannon entropy of the source, and this rate can be matched asymptotically. Here, where the symbol alphabet has size  $\lceil R/q \rceil$ , the entropy is at most  $\log_2(\lceil R/q \rceil)$ . So, for uniform quantization with bin width  $q$ , the cost in bits to store the quantized coefficients can be estimated by  $\#\mathcal{N}_L \log_2(R/q)$ .

We seek to improve on this cost by more effectively distributing the error ‘budget.’ To do this, we quantize the coefficients separately by level. We call this strategy *level-wise quantization*. Suppose the coefficients  $\{u_{\text{mc}}[x] : x \in \mathcal{N}_l^*\}$  are quantized with bin width  $q_l$ . Then

$$\max_{x \in \mathcal{N}_l^*} |u_{\text{mc}}[x] - \tilde{u}_{\text{mc}}[x]| \leq \frac{1}{2} q_l$$

and the estimated cost of encoding the quantization labels for the level is  $\#\mathcal{N}_l^* \log_2(R/q_l)$ . Summing over  $l$ , we define an estimated cost function  $\text{cost}$  by

$$\text{cost}(q_0, \dots, q_L) = \sum_{l=0}^L \#\mathcal{N}_l^* \log_2(R/q_l).$$

Observe that uniform quantization is recovered by using  $q_l = (2\tau/C)/(L+1)$ . The estimated cost agrees with the original expression:

$$\text{cost}\left(\frac{2\tau}{C} \frac{1}{L+1}, \dots, \frac{2\tau}{C} \frac{1}{L+1}\right) = \#\mathcal{N}_L \log_2\left(\frac{R}{\frac{2\tau}{C} \frac{1}{L+1}}\right).$$

Consider the optimization problem

$$\begin{aligned} &\text{minimize} \quad \text{cost}(q_0, \dots, q_L) \\ &\text{subject to} \quad \sum_{l=0}^L \frac{1}{2} q_l = \frac{\tau}{C}. \end{aligned}$$

(The cost decreases as the bin widths increase, so nothing is lost by making the error condition constraint an equality.) A straightforward application of Lagrange multipliers and the convexity of  $\text{cost}$ , which we omit to save space, shows that the solution this problem is given by  $q_l = 2\tau/C \times \#\mathcal{N}_l^*/\#\mathcal{N}_L$ . The estimated cost of this quantization strategy is

$$\text{cost}\left(\frac{2\tau}{C} \frac{\#\mathcal{N}_0^*}{\#\mathcal{N}_L}, \dots, \frac{2\tau}{C} \frac{\#\mathcal{N}_L^*}{\#\mathcal{N}_L}\right) = \sum_{l=0}^L \#\mathcal{N}_l^* \log_2\left(\frac{R}{\frac{2\tau}{C} \frac{\#\mathcal{N}_l^*}{\#\mathcal{N}_L}}\right).$$

The extent to which this is an improvement over the original estimated cost depends on the level sizes  $\#\mathcal{N}_0^*, \dots, \#\mathcal{N}_L^*$ . In a typical grid hierarchy used in MGARD,  $\#\mathcal{N}_l$  scales

like  $2^{ld}$ , with  $d$  the spatial dimension. So, for the sake of illustration, take  $d = 3$ ,  $(\#\mathcal{N}_0, \dots, \#\mathcal{N}_L) = (125, 729, 4913, 35,937, 274,625)$ , and  $CR/2\tau = 250$ . Then the estimated cost is approximately 2,830,000 bits when using uniform quantization and approximately 2,370,000 bits when using level-wise quantization.

## 4.2 Adaptive decomposition

We further propose to perform multi-grid decomposition in adaptive fashion, i.e. stopping at an appropriate level instead of decomposing to end, because we observe that the multi-linear interpolation is not always better than existing de-correlation approaches such as the Lorenzo predictor used in SZ [13], especially when the required error bound becomes tight. On the other hand, the level-wise quantization strategy presented in the previous subsection exponentially decays the error bound for the level coefficients, leading to smaller and smaller error bounds as the number of levels increases. Thus, it is natural to design an adaptive decomposition strategy which stops the multi-grid decomposition at a certain level and switch to more efficient error-controlled compression methods for compressing the remaining coarse representation with high efficiency. In this way, the multi-grid approach is used as a pre-conditioner instead of a standalone compressor.

We select SZ as our external compressor for demonstration purposes, because 1) it is one of the state-of-the-art error-controlled lossy compressors that leads to high compression quality; 2) it yields the best compression ratio given a fixed error bound according to existing studies [13]; and 3) its Lorenzo predictor is complementary to the multi-linear interpolation used in the multi-grid based decomposition in terms of prediction efficiency. Nevertheless, the proposed method can be used on other prediction-based error-controlled lossy compressors such as the hybrid model [9] and high-order Lorenzo predictor [13] which are adept at different regions of the rate-distortion, depending on the actual need from the applications. In the following text, we first discuss the advantages and disadvantages of the Lorenzo predictor used in SZ and the multi-linear interpolation used in the multi-grid decomposition. We will then introduce our error estimation method and the adaptive mechanism to automatically switch between them.

### 4.2.1 Lorenzo versus multi-linear interpolation

Lorenzo predictor [17] estimates the value for a given data point using its immediate neighbors that have already been processed. The data value is predicted by the  $n - 1$  degree polynomials defined by the  $2^n - 1$  neighbor points for  $n$ -dimensional data, and it is proved that the predicted value can be represented as signed combinations of its neighbor nodes. Thus, the neighbor nodes can be divided into two groups: positive nodes with sign coefficient 1 and negative nodes with sign coefficient  $-1$ . For example, as shown in Fig. 1(a), 3D Lorenzo predictor predicts the value for current node with the following formula

$$d_{111}^{(\text{Lo})} = d'_{110} + d'_{101} + d'_{011} - d'_{100} - d'_{010} - d'_{001} + d'_{000}.$$

One major drawback of Lorenzo predictor comes from the inaccurate polynomials computed from the skewed processed data, which leads to unexpected artifacts in the

decompressed data, especially when compression ratio is high (i.e., error bound is loose) [7]. Nevertheless, its high-order function approximation (e.g., quadratic function for 3D data) offers accurate prediction when the impact of decompressed values is small (i.e., error bound is tight) [13].

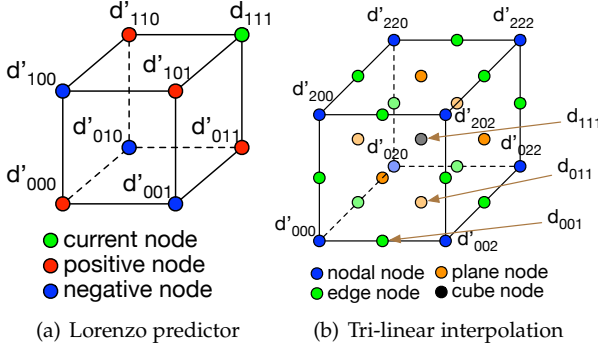


Fig. 1. Illustration of Lorenzo predictor and tri-linear interpolation.

On the other hand, multi-linear interpolation approximates the value of a data point linearly using the available nodal nodes whose value are known (the higher level nodes in case of multi-grid decomposition). Because the multi-grid decomposition uniformly selects half of the nodes in current level as the nodal node, it yields independent prediction for each  $3^n$  grid. For the 3D case illustrated in Fig. 1(b), the 19 coefficient codes within the  $3 \times 3 \times 3$  grid can be classified into 3 main categories: edge nodes which locate on the edge of two nodal nodes (e.g.,  $d_{001}$ ), plane nodes which locate in the middle of four nodal nodes (e.g.,  $d_{011}$ ), and cube nodes which locate in center of eight nodal nodes (e.g.,  $d_{111}$ ). Specifically, the prediction formulas for one example of each category is listed as follows

$$\begin{aligned} d_{001}^{(int)} &= \frac{d'_{000} + d'_{002}}{2} \\ d_{011}^{(int)} &= \frac{d'_{000} + d'_{002} + d'_{020} + d'_{022}}{4} \\ d_{111}^{(int)} &= \frac{d'_{000} + d'_{002} + d'_{020} + d'_{022} + d'_{200} + d'_{202} + d'_{220} + d'_{222}}{8} \end{aligned}$$

Although the multi-linear interpolation will be affected by the skewed decompressed values of nodal nodes as well, it suffers much less than the Lorenzo predictor because of the dividing factor. When the impact of decompressed values decreases (i.e., error bound becomes tighter), the prediction accuracy of multi-linear interpolation is usually not as good as that of Lorenzo predictor because it uses linear approximations. This inspires us to come up with a way to quantify the prediction accuracy of the two approaches while accounting for the impact of decompressed values and adapt to the more appropriate one based on the required error bound for current level.

#### 4.2.2 Penalty estimation

We estimate a penalty factor for the multi-linear interpolation used in the multi-grid decomposition by generalizing the statistical approach from [7]. The penalty factor is defined as the expected difference of prediction with original data and prediction with decompressed data using

the required error bound, which indicates how much the prediction accuracy will be affected by the error bounds. It can also be used to efficiently compare the effectiveness of different prediction methods without quantization (i.e., computing the decompressed data during compression).

Denote  $e$  as the required error bound. Assuming a uniform distribution  $U(-e, e)$  for the errors of decompressed data (which is usually true due to the linear quantization [13]), the penalty factor can be computed via Monte-Carlo simulations. According to [7], 3D Lorenzo predictor yields a penalty factor of  $1.22e$ . Thus, the prediction error of 3D Lorenzo predictor can be estimated with original data and the penalty factor as:

$$E_{\text{Lorenzo}} = |(d_{110} + d_{101} + d_{011} - d_{100} - d_{010} - d_{001} + d_{000}) - d_{111}| + 1.22e.$$

This statistical method can be generalized to multi-linear interpolation in our multi-grid decomposition. Because our method uses linear quantization with level-wise error bounds, we assume two uniform distributions of errors:  $U(-\frac{1}{\kappa}e, \frac{1}{\kappa}e)$  for the nodal nodes (which will be compressed in next level) and  $U(-e, e)$  for the coefficient nodes (which will be compressed in current level), where  $e$  is the error bound of current level and  $\kappa$  is the level-wise quantization factor. Let  $P_{\text{edge}}$ ,  $P_{\text{plane}}$ , and  $P_{\text{cube}}$  be the penalty terms for the coefficient nodes belonging to edge, plane, and, cube nodes, respectively, the penalty terms for multi-grid decomposition turn out to be

$$P_{\text{edge}} = \sum_{i=0}^1 \frac{\epsilon_i}{2}, \quad P_{\text{plane}} = \sum_{i=0}^3 \frac{\epsilon_i}{4}, \quad \text{and} \quad P_{\text{cube}} = \sum_{i=0}^7 \frac{\epsilon_i}{8},$$

where  $\{\epsilon_i\}$  are the random variables indicating the errors of the nodal nodes.

The errors of nodal nodes in multi-grid decomposition compromise of both quantization errors of these nodes and correction errors that are incurred by the quantization errors of coefficient nodes in current level. Using the statistical method, we find that the correction errors for 3D data can be approximated by a Gaussian distribution with 0 means and  $0.8e$  variance when errors of the coefficient nodes are drawn from  $U(-e, e)$ , and they are independent from the number of nodes along each dimension. These correction errors are then added to the quantization errors on nodal nodes, which are drawn from  $U(-\frac{1}{\kappa}e, \frac{1}{\kappa}e)$ , to model the penalty. Based on our experiments, the penalty factors for coefficient nodes in the three categories on 3D datasets are  $E(|P_{\text{edge}}|) = 0.518e$ ,  $E(|P_{\text{plane}}|) = 0.366e$ , and  $E(|P_{\text{cube}}|) = 0.259e$ , respectively. Accordingly, the prediction error of the multi-grid based approach for node  $d_{111}$  in Fig. 1(b) can be estimated as:

$$E_{\text{interp}} = \left| \frac{1}{8} (d_{000} + d_{002} + d_{020} + d_{022} + d_{200} + d_{202} + d_{220} + d_{222}) - d_{111} \right| + 0.259e,$$

With the computed penalty factors, we can use the original data to estimate the prediction accuracy of the two methods without performing the time-consuming quantization. We can also infer that Lorenzo predictor will be affected more than the multi-linear interpolation by using decompressed value because it has a larger constant in the penalty factor, which is consistent with our observation that Lorenzo predictor suffers more on loose error bounds.

### 4.2.3 Adaptive decomposition based on error estimation

We then use a sampling approach to determine the most appropriate decomposition level according to the accuracy of the two prediction methods. In particular, we uniformly sample the data in current level in the granularity of  $3^n$  blocks and estimate the prediction errors of coefficient nodes for both Lorenzo predictor and multi-linear interpolation. Note that we need to apply the penalty factors computed above to account for the impact of decompressed values. In our implementation, we sample one out of four blocks along each dimension and accumulate the estimated prediction error for different methods. If the accumulated prediction error of Lorenzo predictor is less than that of multi-linear interpolation, we will compress all the data in current level using SZ (which uses Lorenzo predictor); otherwise, we will continue to perform multi-grid decomposition.

## 5 IMPLEMENTATION AND OPTIMIZATIONS

Besides quality, performance is another important aspect for large-scale scientific data compression. We implement our multi-grid based data decomposition/recomposition framework with a series of optimizations to achieve high performance and high efficiency. As decomposition and recomposition are the key steps for both data refactoring and data reduction, optimizing their performance leads to improved performance for both the two aspects.

### 5.1 Level-centric data reorder

We leverage a data reorder algorithm to deal with the strided memory access in the multi-grid method, inspired by the de-interleaving phase in wavelet decomposition. Specifically, we rearrange the input data in a level-centric manner to cluster data to be used in next level together, such that the memory access in the next level could be coherent as well. In what follows, we first identify the data dependency and memory access patterns in the multigrid decomposition and introduce the reorder algorithm thereafter.

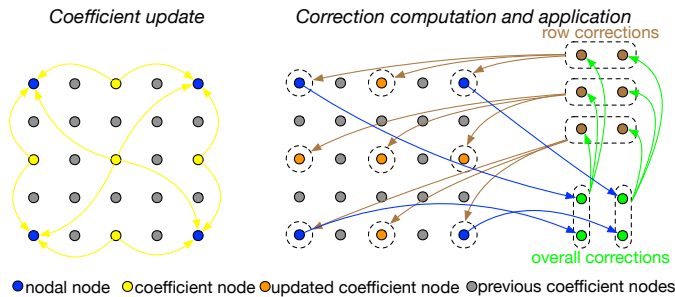


Fig. 2. Strided data dependency in the multigrid method (level = 1).

As mentioned in Section 2, *coefficient computation*, *correction computation*, and *correction application* are the key modules used in the multigrid method. We illustrate the strided data dependencies for operations in these modules using a 2D example shown in Fig. 2. In each iteration, *coefficient computation* computes the multi-linear interpolations for all the coefficient nodes using their adjacent nodal nodes in current level, and updates the values of these coefficient nodes with the difference between their original values and the

computed interpolations. After that, *correction computation* will perform a row sweep to compute the row correction, followed by a column sweep on the resulting row correction to obtain the overall correction. At last, the overall correction will be applied to the nodal values in the *correction application*. As we can see from the figure, almost all the operations here involve strided memory access which skips the processed nodes, leading to inefficient cache utilization because values of processed nodes are fetched but never referenced. Furthermore, a stride large than the number of elements that a cacheline can hold will result in cache misses everywhere. In other words, only the first level of the multigrid decomposition makes efficient use of the cache.

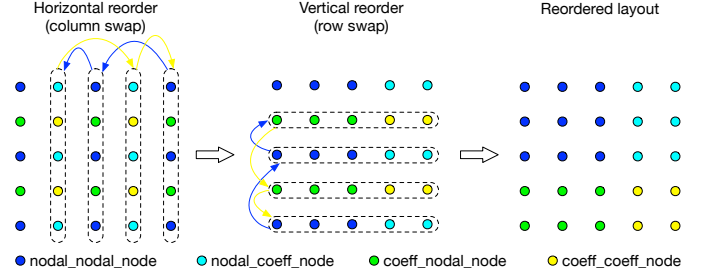


Fig. 3. 2D data reorder.

To enable efficient cache utilization, we reorder the data in order to cluster the nodal nodes (i.e., the nodes that will be used for next level decomposition) in current level together. We implement this by a horizontal reorder and a vertical reorder. In a 2D grid with dimensions  $(2n_1 + 1) \times (2n_2 + 1)$ , the horizontal reorder essentially moves the  $(2i + 1)$ -th column to the  $i$ -th column and  $2i$ -th column to  $(2i + 1)$ -th column, where  $i$  ranges from 1 to  $n_2$ , such that the nodal columns are moved together. Then, the vertical reorder applies similar operations to the rows in order to cluster the nodal rows together. Denote *nodal\_nodal\_node* as nodes in both nodal rows (i.e. rows that will be present in next level representation) and *nodal* columns (i.e. columns that will be present in next level representation), *nodal\_coeff\_node* as nodes in nodal rows but coefficient columns (i.e. columns that will be absent in next level representation), *coeff\_nodal\_node* as nodes in coefficient rows (i.e. rows that will be absent in next level representation) but nodal columns, and *coeff\_coeff\_node* as nodes in both coefficient rows and coefficient columns. Fig. 3 shows how the reorder algorithm works for  $5 \times 5$  2D data.

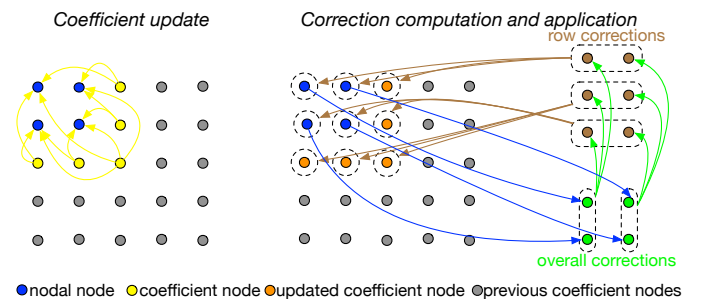


Fig. 4. Reordered data dependency (level = 1).

Fig. 4 shows the data dependencies in the multigrid



method after reorder. Compared with original data, the reordered data requests memory access in a more contiguous way, which promises higher performance.

Given the reordered data, we then perform sliding window update for efficient coefficient computation. Specifically, we locate the starting positions of different groups of nodes (e.g., nodal\_nodal\_node, nodal\_coeff\_node, coeff\_nodal\_node, and coeff\_coeff\_node for the 2D case), and compute their coefficients simultaneously. In this way, coefficient computation can be done for only one pass of the data in current level with good cache utilization.

During recomposition, data is already ordered in a level-centric manner. In this case, we perform correction computation, correction recover, and coefficient recover on the ordered data directly, followed by an inverse reorder operation to put recomposed data to the correct positions of the finer level.

## 5.2 Direct load vector computation

We then optimize the load vector computation, which is an important step in obtaining the correction  $Q_{l-1}(I - \Pi_{l-1})Q_l u$ . Load vector is defined as the function expressed in terms of nodal displacements, and its  $i$ -th element is computed by the inner product of the multilevel component  $(I - \Pi_{l-1})Q_l u$  and the  $i$ -th nodal basis function  $\phi_l^i$  in next level

$$f_i = ((I - \Pi_{l-1})Q_l u, \phi_l^i).$$

The previous multi-grid approach [11] computes the load vector in multi-dimensional cases by multiplying the fine grid mass matrix by the computed coefficients followed by a restriction transform to the coarse grid, i.e.  $((I - \Pi_{l-1})Q_l u, \phi_l^i) = R_l M_l \alpha$ , where  $R_l$  is a transfer matrix for nodal basis such that  $\phi_{l-1} = R_l \phi_l$ ,  $M_l$  is the mass matrix, and  $\alpha$  is the vector of nodal values of the multilevel coefficient  $(I - \Pi_{l-1})Q_l u$ . The computed load vector will then be used to compute the correction  $z_l$  by solving the linear system  $M_l z_l = f$ . This approach requires two passes of data, namely multiplying mass matrix  $M_l$  and applying the transfer matrix  $R_l$ .

We generalize the derivation for load vector in one-dimensional case in [10] to multi-dimensional cases so that only one pass of data access is needed. Although the multi-dimensional load vector computation boils down to multiple one-dimensional computations along each dimension, it is not exactly the same as that of one-dimensional cases as displayed in Fig. 5. Specifically, non-zero values of  $(I - \Pi_{l-1})Q_l u$  only appear on the coefficient nodes in one-dimensional case, because the difference between original value and interpolation on nodal nodes are 0. However, it is not the case for multi-dimensional data because the coefficient nodes may be nodal nodes along a certain dimension during the computation (e.g., nodal\_coeff nodes in Fig. 3). To tackle this issue, we generalize load vector computation with the following lemma.

**Lemma 1.** Denote the values of nodes in current level as  $c_0, c_1, \dots, c_{2n+1}$  as shown in Fig. 5. Further denote  $c_{-1} = c_{2n+2} = 0$  and the uniform-spacing interval

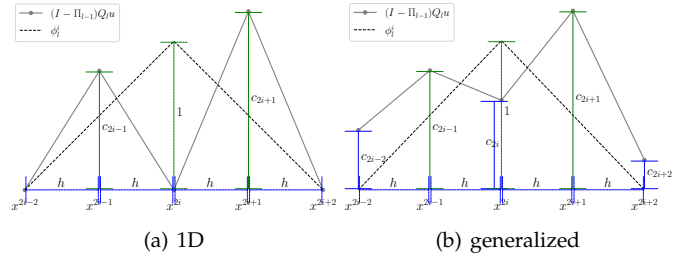


Fig. 5. 1D and generalized load vector computation.

length as  $h$ , the  $i$ -th entry of the load vector in generalized case can be computed by

$$f_i = (\frac{1}{12}c_{2i-2} + \frac{1}{2}c_{2i-1} + \frac{5}{6}c_{2i} + \frac{1}{2}c_{2i+1} + \frac{1}{12}c_{2i+2})h.$$

*Proof:* The entries of load vector are calculated via the integral of the piece-wise linear interpolations with nodal nodes and the corresponding nodal basis functions in the coarse grid. It can be decomposed into the integrals of four separate regions and computed as follows:

$$\begin{aligned} l[i] &= \int_{-2h}^{-h} \frac{x+2h}{2h} \frac{c_{2i-1}(x+2h) + c_{2i-2}(-h-x)}{h} dx \\ &+ \int_{-h}^0 \frac{x+2h}{2h} \frac{c_{2i}(x+h) + c_{2i-1}(-x)}{h} dx \\ &+ \int_0^h \frac{2h-x}{2h} \frac{c_{2i+1}x + c_{2i}(h-x)}{h} dx \\ &+ \int_h^{2h} \frac{2h-x}{2h} \frac{c_{2i+2}(x-h) + c_{2i+1}(2h-x)}{h} dx \\ &= (\frac{1}{12}c_{2i-2} + \frac{1}{2}c_{2i-1} + \frac{5}{6}c_{2i} + \frac{1}{2}c_{2i+1} + \frac{1}{12}c_{2i+2})h \end{aligned}$$

□

When the nodal values  $\{c_{2i}\}$  are all 0, the lemma degrades to the one-dimensional case mentioned in [10].

## 5.3 Batch correction computation

We use batch operations to further improve the memory access efficiency for the intermediate corrections in addition to that for the node values optimized in Section 5.1. As indicated by the green arrows in Fig. 2 and Fig. 4, the column sweep that computes the load vector and solves the corresponding tri-diagonal linear system for each separate column of the computed row corrections requires strided memory access. This problem is exacerbated on 3D datasets, which call for such memory access patterns along two discontinuous dimensions. Fortunately, the column sweep needs to be applied to all the columns in the current level and thus can be optimized through batch operations. Specifically, denote batchsize as  $b$ , we perform *direct load vector computation* simultaneously on  $b$  contiguous nodes which are the first ones across multiple columns, and proceed to next  $b$  nodes. In other words, the  $i$ -th entries of the load vectors for different columns are computed together to achieve efficient cache utilization. After that, a slightly modified Thomas algorithm is used to solve the tri-diagonal linear systems in batch.

This optimization requires  $\frac{b \max n_i}{\prod_i n_i}$  auxiliary memory to store the column load vectors, where  $n_i$  is the number of data points along the  $i$ -th dimension. Because batchsize  $b$  is usually small, such memory overhead is indeed negligible for multi-dimensional cases. In our experiments, we observe that `batchsize` = 16 already yields good performance that is similar to that of any larger batch sizes. To account for variations on different systems while limiting memory overhead, we use `batchsize` = 32 as our default configuration.

### 5.4 Intermediate variable elimination & reuse

We identify and eliminate the common multipliers as well as repeat computation of intermediate variables in the multi-grid algorithm for more efficient computation.

First, we found that the interval length  $h$  (which is also the level stride) is the common multiplier in the tri-diagonal linear system solving for correction computation. Specifically, the target linear system can be written as follows

$$\begin{bmatrix} \frac{2}{3}h & \frac{2}{3}h & 0 & \dots & 0 & 0 & 0 \\ h & h & \frac{2}{3}h & \dots & 0 & 0 & 0 \\ 0 & \frac{2}{3}h & \frac{4}{3}h & \dots & 0 & 0 & 0 \\ \vdots & \vdots & \vdots & \ddots & \vdots & \vdots & \vdots \\ 0 & 0 & 0 & \dots & \frac{2}{3}h & \frac{4}{3}h & \frac{2}{3}h \\ 0 & 0 & 0 & \dots & 0 & \frac{2}{3}h & h \end{bmatrix} \begin{bmatrix} z_l^0 \\ z_l^1 \\ z_l^2 \\ \vdots \\ z_l^{n-2} \\ z_l^{n-1} \end{bmatrix} = \begin{bmatrix} f_0h \\ f_1h \\ f_2h \\ \vdots \\ f_{n-2}h \\ f_{n-1}h \end{bmatrix},$$

where  $h$  is the level stride,  $f_i$  is the coefficient of load vector entries, and  $z_l$  is the correction to be applied to the nodal nodes. Thus, the common multiplier  $h$  can be extracted and cancelled from the mass matrix generation and load vector computation, which saves the computational cost.

We also reuse the intermediate variables to avoid repeated computation, where the auxiliary arrays used in solving the tri-diagonal linear systems are typical examples. Because the tri-diagonal mass matrix is fixed for each dimension, we compute the related auxiliary arrays at the very beginning of the multigrid decomposition/recomposition algorithm and pass the pre-computed results as arguments. This adjustment reduces the computational complexity on these variables from  $O(\prod_{i=0}^d n_i)$  to  $O(\sum_{i=0}^d n_i)$ , with merely  $\sum_{i=0}^d n_i$  additional memory.

## 6 EVALUATION

In this section, we present the performance evaluation results to demonstrate the effectiveness of our methods for scientific data management in terms of data reduction and refactoring. Specifically, we compare both compression/decompression performance and rate-distortion of our method with four state-of-the-art error-bounded lossy compressors — MGARD [11], SZ [7], ZFP [3], and the hybrid model proposed in [9] — using four real-world datasets from Scientific Data Reduction Benchmarks [18]. We further show how our approach improves the efficiency of scientific analysis using the iso-surface mini-application widely used in scientific visualization.

### 6.1 Experimental Setup

We conducted our experimental evaluations on the Rhea cluster [19] at Oak Ridge National Laboratory. Each node on

the systems has two 8-core Intel Xeon E5-2650 processors and 128 GB of memory. All the compressors we benchmarked are their latest releases as of Sep. 1st, 2020. They are compiled with gcc-4.8.5 which is the default compiler provided in the cluster. The datasets we use for evaluation are from multiple domains, including Hurricane Isabel climate simulation [20], NYX cosmology simulation [21], and SCALE-LETKF weather simulation [22], and QMCPACK [23] which is quantum Monte Carlo simulation. The details of the datasets are listed in Table 1. Note that the data size in the table only accounts for data in a single core. The total data size goes up to 2.4 TB, 6 TB, 12.6 TB, and 1.2 TB when 2k cores are used in our scalability evaluation.

TABLE 1  
Datasets for evaluation

	#Fields	Dimensions	Size
Hurricane Isabel	13	100 × 500 × 500	1.21 GB
NYX	6	512 × 512 × 512	3 GB
SCALE-LETKF	12	98 × 1200 × 1200	6.31 GB
QMCPACK	1	288 × 115 × 69 × 69	0.59 GB

### 6.2 Performance

We first evaluate the performance of our framework in terms of both decomposition/recomposition and compression/decompression. Specifically, we show the performance improvement on decomposition/recomposition from the proposed optimizations with detailed breakdown, and how it can be used to accelerate scientific data analytics. After that, we compare the overall compression/decompression among the state-of-the-art error-controlled lossy compressors. At last, we conduct a parallel experiment to demonstrate the scalability of the algorithm.

#### 6.2.1 Decomposition/recomposition

Fig. 6 illustrates the decomposition/recomposition performance improvement of our framework with respect to the optimizations in Section 5 when compared with existing approach (the blue bar in the figure). DR, DLVC, BCC, IVER are the abbreviations for data reorder (Section 5.1), direct load vector computation (Section 5.2), batched correction computation (Section 5.3), and intermediate variable elimination/reuse (Section 5.4), respective. We evaluate the impact of DLVC, BCC, and IVER by including them progressively (the orange bar, the green bar, and the red bar in the figure) in addition to DR.

From this figure, we observe that the optimizations adopted in our framework significantly improve the efficiency of the multi-grid method for both decomposition and recomposition. In absolute terms, the final decomposition performance of our framework is 20×, 28×, 39× and 71× than that of the existing multigrid implementation on the four datasets, respectively. Similarly, the recomposition performance of our framework is over 22×, 30×, 41× and 80× than that of the existing implementation. These performance improvements demonstrate the high efficiency of the proposed optimizations.



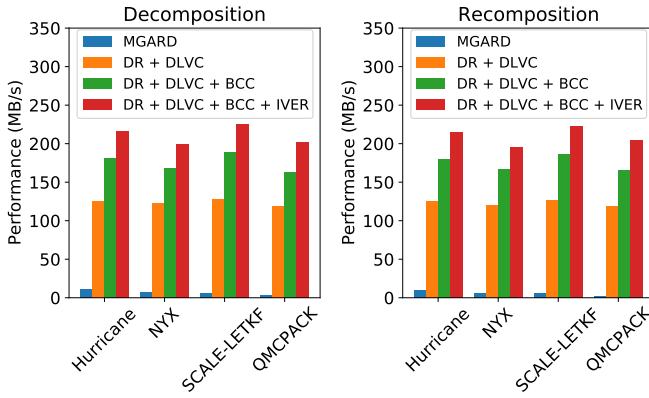


Fig. 6. Decomposition/recomposition performance with optimizations.

### 6.2.2 Use case: accelerating iso-surface computation

We further show how our method benefits scientific analysis by performing the analysis on the decomposed representations, using iso-surface extraction in scientific visualization as an example. An iso-surface is a three-dimensional analog of an iso-line. It is a surface that represents points of a constant value (i.e., iso-value) within a volume of space, which can be used to study specific features around objects, such as features of fluid flows around aircraft wings in computational fluid dynamics. In what follows, we first show the accuracy of iso-surface computation using MGARD and our method with different levels of hierarchical representations. After that, we demonstrate the performance improvement of conducting analysis with coarse representations.

We use the area of the computed iso-surface, which is the outcome of the analysis, to measure the accuracy of different representations. Two representative fields (velocity\_x and temperature) from NYX datasets are evaluated with designated iso-values. The iso-value is set to 0 for velocity\_x because there are specific property scientists would like to see when velocity equals 0. As for temperature, the iso-value is set to the mean of data. Table 2 and Table 3 display the relative errors on the area of iso-surface for the designated iso-value. From the two examples, we can see that our method has similar error compared with MGARD, but offers significantly higher decomposition/recomposition performance. Specifically, they both have less than 7% error for the level 3 presentations, which could be enough for domain scientists in certain cases.

TABLE 2  
Relative error on iso-surface area and decomposition performance (NYX velocity\_x)

	Level	1	2	3
Rel. Error	MGARD	1.61%	0.07%	5.23%
	OurMethod	1.65%	0.10%	5.21%
Perf. (MB/s)	MGARD	8.95	7.27	6.90
	OurMethod	226.63	203.72	202.67

Fig. 7 displays the overall time spending on analysis for MGARD and our method, which includes both time for decomposition and time for conducting analysis on the decomposed representation. The black dash line indicates

TABLE 3  
Relative error on iso-surface area and decomposition performance (NYX temperature)

	Level	1	2	3
Rel. Error	MGARD	5.72%	7.58%	6.86%
	OurMethod	5.79%	7.64%	6.89%
Perf. (MB/s)	MGARD	8.69	7.04	6.68
	OurMethod	226.39	204.60	202.66

the time for performing the analysis on original data, and the green and red dash line show the time of conducting strong-scaling experiments with 8 cores and 64 cores, respectively. It is observed that MGARD suffers from high decomposition overhead, which leads to minor performance gain (temperature) and may even be more costly when the analysis is fast (velocity\_x). On the other hand, our method significantly improves the performance of the scientific analysis: performing the analysis on level 3 representation with single core can lead to comparable performance to that of strong-scaling with 64 cores. Also, such performance gain would be more significant when multiple iso-values need to be computed (i.e. the analysis becomes more expensive).

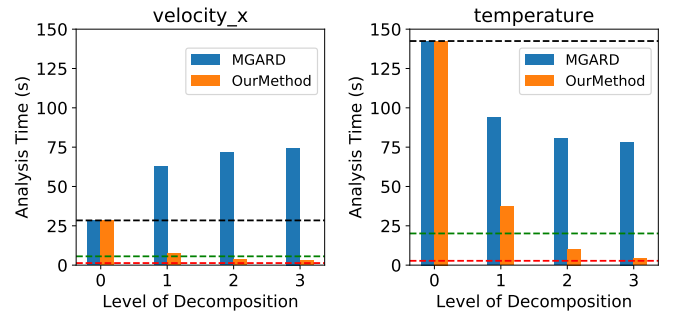


Fig. 7. Overall analysis time (decomposition time + analysis time on reduced representation) of iso-surface evaluation on two representative fields in the NYX dataset. Dashed lines indicate the strong-scaling result of performing iso-surface analysis with 1 core (black), 8 cores (green) and 64 cores (red).

### 6.2.3 Compression/decompression

Besides the decomposition/recomposition performance, we show the end-to-end compression/decompression performance our method and compare it with state-of-the-art lossy compressors in Fig. 8. According to this figure, ZFP leads all the compressors in terms of both compression and decompression performance, but its advantage decreases as error bound becomes tighter. Our method significantly improves the performance of MGARD, leading to compression performance comparable to that of SZ. The decompression performance of our method is lower than SZ, because decompression in our approach is as costly as compression due to the symmetric operations while SZ has higher decompression performance than compression performance. The hybrid model has higher decompression performance than our method, but its compression performance is only one half that of our method in most cases.

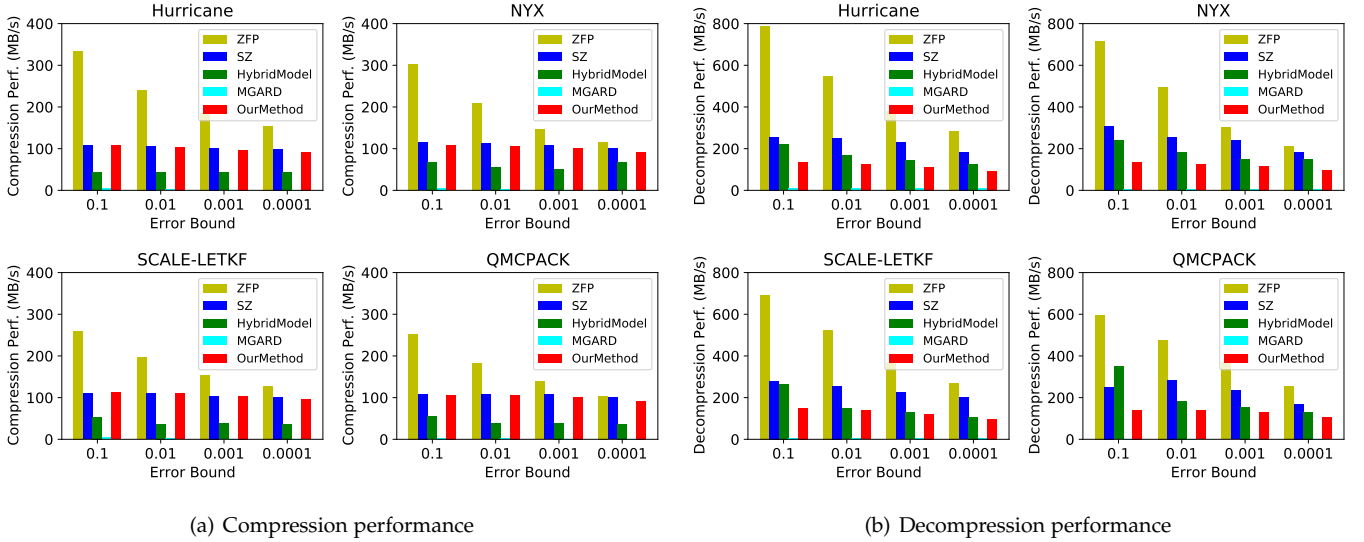


Fig. 8. Compression/decompression performance of the error-bounded lossy compressors.

### 6.2.4 Scalability

Because most data compression methods are designed in an embarrassingly parallel fashion, they are expected to have linear speedup when executed in parallel. We validate this by evaluating our method on 512, 1024, and 2048 cores, respectively, with error bound 0.001 for demonstrate purposes. This corresponds to 2.4 TB, 6 TB, 12.6 TB, and 1.2 TB of data with respect to the four datasets when 2k cores are used. As shown in Fig. 9, we observe almost linear speedup for both compression and decompression, which demonstrates the scalability of embarrassingly parallel data compression methods. Such characteristics promise high throughput when scale increases, which is very important for exascale data management.

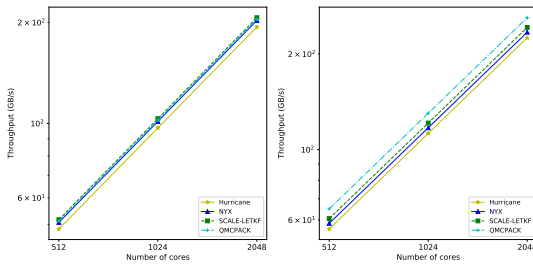


Fig. 9. Scalability of the proposed compression method.

## 6.3 Compression quality

We then evaluate compression quality in terms of rate-distortion as introduced in Section 3. In what follows, we first evaluate the effect of the proposed techniques, namely level-wise quantization and adaptive decomposition, and compare our method with existing error-controlled lossy compressors.

### 6.3.1 Impact of level-wise quantization and adaptive decomposition

We present the impact of the proposed techniques in Fig. 10. The cyan line in this figure shows the rate-distortion of

MGARD with uniform quantization across levels and extensive decomposition, which the baseline. The yellow line (LQ) and green line (AD) display the rate-distortions after independently applying the level-wise quantization strategy proposed in Section 4.1 and adaptive decomposition strategy introduced in Section 4.2, respectively. We also include the rate-distortion of SZ (the blue line) as another baseline for adaptive decomposition strategy. The red line illustrates the result of our method, which incorporates both level-wise quantization and adaptive decomposition.

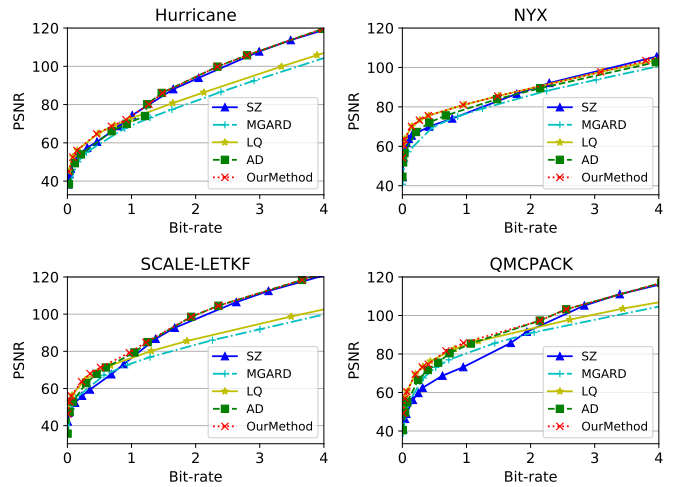


Fig. 10. Impact of level-wise quantization and adaptive decomposition on rate-distortion.

From this figure, we can observe that both level-wise quantization (LQ) and adaptive decomposition (AD) have stable improvements over MGARD on all bit-rates with different emphasizes. Specifically, level-wise quantization provides more advantages in small bit-rates (e.g., [0, 1]) while adaptive decomposition is more adept at large bit-rates (e.g., [1, 4]). This is consistent with our analysis in Section 4.2: multi-linear interpolation leveraged by level-wise quantization is more efficient for large error bounds

(i.e., small bit-rates) but less efficient for small error bounds (i.e., large bit-rates) compared with the Lorenzo predictor used in SZ. In large bit-rates when Lorenzo predictor is always better, the approaches with adaptive decomposition degrade to SZ because they switch the prediction method at the very first level. Our final solution, which integrates and takes advantages of both two strategies, yields the best rate-distortion on all the four datasets.

### 6.3.2 Comparison with state-of-the-art compressors

We then compare the rate-distortion of our solution with the four state-of-the-art error-controlled lossy compressors mentioned before in Fig. 11 and Fig. 12. We present the rate-distortion of bit-rate in  $[0, 4]$ , which corresponds to compression ratios  $\geq 8$ , and an enlarged view of bit-rate in  $[0, 1]$ , or equivalently compression ratios  $\geq 32$ . According to this figure, our method leads to the rate-distortion at most bit-rates in most of the datasets. The only exception is QMCPACK, where both the multi-linear interpolation in the multi-grid decomposition and Lorenzo predictor in SZ are not as good as the transform-based decorrelation method used in ZFP and the hybrid model when bit-rate goes up. Nevertheless, our method can adapt to such scenario as well by using either ZFP or the hybrid model as our external compressor in adaptive decomposition, which is our future work. In addition, our method significantly improves the rate-distortion of QMCPACK in bit-rate range  $[0, 1]$  as shown in Fig. 12, thanks to the level-wise quantization. Also, it is interesting to notice that the improvement of our method over the second best lossy compressor is large on QMCPACK in bit-rate range  $[0, 1]$ , but less on NYX and SCALE-LETKF, and minor on Hurricane. This is most likely caused by the characteristics of the datasets: data in QMCPACK is the most smooth so they could be better represented by the multi-linear interpolation in the multi-grid method while data in Hurricane may be the most varying thus cannot be model very well by such technique.

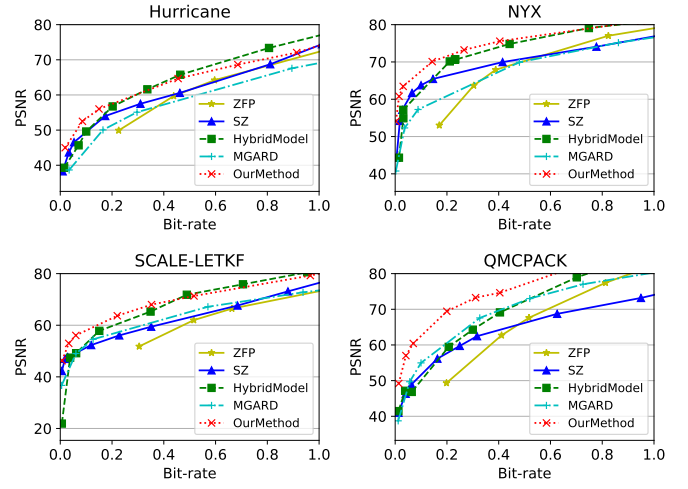


Fig. 12. Rate-distortion of error-controlled lossy compressors on the four datasets. (bit-rate  $\in [0, 1]$ )

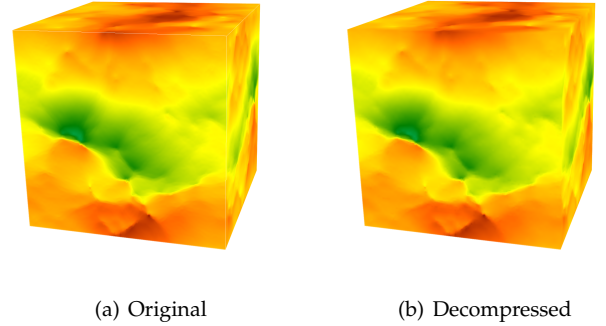


Fig. 13. Visualization of original data and decompressed data using our method (NYX velocity\_x, dataset PSNR = 60.12, compression ratio = 2525, field PSNR = 57.37, compression ratio = 1396).

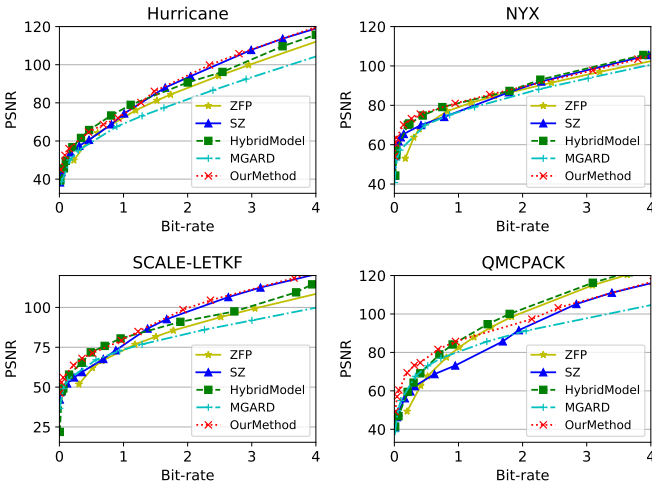


Fig. 11. Rate-distortion of error-controlled lossy compressors on the four datasets. (bit-rate  $\in [0, 4]$ )

We further show the compression ratios and performance of the evaluated error-controlled lossy compressors

on the four dataset when tuning them to have almost the same distortion in Table 4. We use a PSNR of around 60 for demonstration purposes, because such PSNR is able to provide valid data for visualization purposes. Fig. 13 visualizes the original data of NYX velocity\_x field, as well as the decompressed data using our compression method, which shows almost no difference visualization even under such a high compression ratio. Although our method is slower than ZFP in terms of performance, but it offers  $2\times \sim 20\times$  improvements on the compression ratios under the same distortion. Also, our method has similar compression performance compared to that of SZ, which is almost  $2\times$  as fast as the hybrid model in most cases. Generally speaking, our method has up to  $2\times$  compression improvement over that of the best existing methods, which could be a very good option to reduce the storage requirement and I/O intensity for exascale systems.

## 7 RELATED WORKS

Storage limitation and I/O bottleneck have become serious problems for large-scale scientific applications. Data com-

TABLE 4  
Compression ratios (CR) and performance (Perf.) when PSNR  $\approx$  60

Datasets	Compressors	PSNR	CR	Perf. (MB/s)
Hurricane	SZ	59.97	74.08	105.02
	ZFP	59.68	73.01	335.63
	HybridModel	59.99	110.66	43.73
	OurMethod	60.21	<b>120.08</b>	96.03
NYX	SZ	59.84	722.72	115.84
	ZFP	59.44	130.44	346.47
	HybridModel	59.20	834.49	87.95
	OurMethod	60.12	<b>2525.93</b>	94.23
SCALE-LETKF	SZ	59.42	91.1	108.22
	ZFP	57.49	79.14	287.78
	HybridModel	59.38	176.38	57.78
	OurMethod	59.82	<b>252.53</b>	104.82
QMCPACK	SZ	59.73	128.26	106.11
	ZFP	57.76	99.08	291.72
	HybridModel	59.53	148.09	39.70
	OurMethod	60.42	<b>467.85</b>	100.30

pression is a direct way to address such problems, and many approaches have been proposed and developed in literature.

Lossless compressors [24], [25], [26], [27] are developed to recover exact data while reducing the size, but they only afford limited compression ratio for the floating-point scientific data. According to recent studies [28], their compression ratios are usually less than 3, which is not able to meet the demand from today's large-scale scientific simulations and experimental devices.

Error-bounded lossy compression [2], [3], [4], [5], [6], [7], [8], [9] is proposed to trade off data accuracy for compression ratio, which features in offering high compression ratios while controlling data distortion. General error-bounded lossy compressors can be divided into two categories, namely prediction-based ones and transform-based ones, based on how they decorrelate original data. Prediction-based lossy compressors such as [2], [7], [9] leverage prediction models to decorrelate original data, while transform-based ones such as [3] rely on invertible transforms to do so. According to previous work [29], SZ [7] and ZFP [3] are the two best error-bounded lossy compressors of their kinds. They usually lead to higher compression quality under the same distortion when compared with other approaches. A previous approach [9] proposed to use transform-based compressors as a predictor for better compression quality, but it suffered from high overhead in terms of performance because of a costly iterative sampling strategy for best-fit predictor selection. Another approach [30] tried to select the better one between the best of SZ and ZFP, but it at most provides the same compression quality as either SZ or ZFP.

Recently, multigrid-based data reduction [10], [11], [12] has been proposed by the applied math community as a brand new method for error-bounded lossy compression. However, it is not able to provide comparable reduction performance and quality compared with others for regular mesh data. In this work, we leverage the multigrid-based framework that we design and implement to improve the reduction performance for this approach. Furthermore, after carefully studying the error distribution, we propose to use this method as a preconditioner rather than a stand-alone compressor for data reduction, which outperforms existing approaches in terms of rate-distortion. To the best of our

knowledge, this is the first attempt to combine multigrid-based data reduction method with other compressors to form a new error-bounded lossy compressor.

## 8 CONCLUSION

In this paper, we present two novel techniques to enhance the compression quality of multi-grid based data reduction, as well as a series of optimizations to improve the performance. The proposed approach leads to up to  $2\times$  compression ratio gain compared to state-of-the-art error-controlled lossy compressors under the same distortion and tens of performance improvement over the existing multi-grid based implementation. In the future work, we plan to further improve the quality of multi-grid based data reduction by exploring higher-order basis functions and adapt them in different regions of data.

## REFERENCES

- [1] M. S. Summers, G. Alvarez, J. Meredith, T. A. Maier, and T. C. Schultness, "DCA++: A case for science driven application development for leadership computing platforms," in *Journal of Physics: Conference Series*, vol. 180, no. 1. IOP Publishing, 2009, p. 012077.
- [2] S. Di and F. Cappello, "Fast error-bounded lossy HPC data compression with SZ," in *2016 IEEE International Parallel and Distributed Processing Symposium*. IEEE, 2016, pp. 730–739.
- [3] P. Lindstrom, "Fixed-rate compressed floating-point arrays," *IEEE Transactions on Visualization and Computer Graphics*, vol. 20, no. 12, pp. 2674–2683, 2014.
- [4] P. Lindstrom and M. Isenburg, "Fast and efficient compression of floating-point data," *IEEE Transactions on Visualization and Computer Graphics*, vol. 12, no. 5, pp. 1245–1250, 2006.
- [5] S. Lakshminarasimhan, N. Shah, S. Ethier, S.-H. Ku, C.-S. Chang, S. Klasky, R. Latham, R. Ross, and N. F. Samatova, "Isabela for effective in situ compression of scientific data," *Concurrency and Computation: Practice and Experience*, vol. 25, no. 4, pp. 524–540, 2013.
- [6] Z. Chen, S. W. Son, W. Hendrix, A. Agrawal, W.-k. Liao, and A. Choudhary, "NUMARCK: machine learning algorithm for resiliency and checkpointing," in *Proceedings of the International Conference for High Performance Computing, Networking, Storage and Analysis*. IEEE Press, 2014, pp. 733–744.
- [7] X. Liang, S. Di, D. Tao, S. Li, S. Li, H. Guo, Z. Chen, and F. Cappello, "Error-controlled lossy compression optimized for high compression ratios of scientific datasets," in *2018 IEEE International Conference on Big Data*. IEEE, 2018.
- [8] X. Liang, S. Di, D. Tao, Z. Chen, and F. Cappello, "Efficient transformation scheme for lossy data compression with point-wise relative error bound," in *IEEE International Conference on Cluster Computing (CLUSTER)*, 2018, pp. 179–189.
- [9] X. Liang, S. Di, S. Li, D. Tao, B. Nicolae, Z. Chen, and F. Cappello, "Significantly improving lossy compression quality based on an optimized hybrid prediction model," in *Proceedings of the International Conference for High Performance Computing, Networking, Storage and Analysis*, 2019, pp. 1–26.
- [10] M. Ainsworth, O. Tugluk, B. Whitney, and S. Klasky, "Multilevel techniques for compression and reduction of scientific data—the univariate case," *Computing and Visualization in Science*, vol. 19, no. 5–6, pp. 65–76, 2018.
- [11] —, "Multilevel techniques for compression and reduction of scientific data—the multivariate case," *SIAM Journal on Scientific Computing*, vol. 41, no. 2, pp. A1278–A1303, 2019.
- [12] —, "Multilevel techniques for compression and reduction of scientific data—quantitative control of accuracy in derived quantities," *SIAM Journal on Scientific Computing*, vol. 41, no. 4, pp. A2146–A2171, 2019.
- [13] D. Tao, S. Di, Z. Chen, and F. Cappello, "Significantly improving lossy compression for scientific data sets based on multidimensional prediction and error-controlled quantization," in *2017 IEEE International Parallel and Distributed Processing Symposium*. IEEE, 2017, pp. 1129–1139.

- [14] T. Berger, "Rate-distortion theory," *Wiley Encyclopedia of Telecommunications*, 2003.
- [15] C. C. for Online Data Analysis and Reduction, "MGARD," <https://github.com/CODARcode/MGARD>, October 2020, accessed 2020-10-09.
- [16] C. E. Shannon, "A mathematical theory of communication," *SIG-MOBILE Mob. Comput. Commun. Rev.*, vol. 5, no. 1, pp. 3–55, Jan. 2001.
- [17] L. Ibarria, P. Lindstrom, J. Rossignac, and A. Szymczak, "Out-of-core compression and decompression of large n-dimensional scalar fields," in *Computer Graphics Forum*, vol. 22, no. 3. Wiley Online Library, 2003, pp. 343–348.
- [18] Scientific Data Reduction Benchmark, <https://sdrbench.github.io/>, 2019, online.
- [19] Rhea, Available at <https://www.olcf.ornl.gov/olcf-resources/compute-systems/rhea>, online.
- [20] Hurricane ISABEL simulation data, <http://vis.computer.org/vis2004contest/data.html>, 2019, online.
- [21] NYX simulation, <https://amrex-astro.github.io/Nyx>, 2019, online.
- [22] S.-L. weather model, <https://github.com/gylien/scale-letkf>, 2019, online.
- [23] J. Kim, A. D. Baczewski, T. D. Beaudet, A. Benali, M. C. Bennett, M. A. Berrill, N. S. Blunt, E. J. L. Borda, M. Casula, D. M. Ceperley, S. Chiesa, B. K. Clark, R. C. Clay, K. T. Delaney, M. Dewing, K. P. Esler, H. Hao, O. Heinonen, P. R. C. Kent, J. T. Krogel, I. Kylänpää, Y. W. Li, M. G. Lopez, Y. Luo, F. D. Malone, R. M. Martin, A. Mathuriya, J. McMinis, C. A. Melton, L. Mitas, M. A. Morales, E. Neuscamman, W. D. Parker, S. D. P. Flores, N. A. Romero, B. M. Rubenstein, J. A. R. Shea, H. Shin, L. Shulenburger, A. F. Tillack, J. P. Townsend, N. M. Tubman, B. V. D. Goetz, J. E. Vincent, D. C. Yang, Y. Yang, S. Zhang, and L. Zhao, "QMCPACK: an open source ab initio quantum Monte Carlo package for the electronic structure of atoms, molecules and solids," *Journal of Physics: Condensed Matter*, vol. 30, no. 19, p. 195901, 2018.
- [24] F. Altred, "Blosc, an extremely fast, multi-threaded, meta-compressor library," 2017.
- [25] M. Burtcher and P. Ratanaworabhan, "FPC: A high-speed compressor for double-precision floating-point data," *IEEE Transactions on Computers*, vol. 58, no. 1, pp. 18–31, Jan 2009.
- [26] L. P. Deutsch, "GZIP file format specification version 4.3," 1996.
- [27] Zstd, <https://github.com/facebook/zstd/releases>, 2019, online.
- [28] P. Lindstrom, "Error distributions of lossy floating-point compressors," *Joint Statistical Meetings*, pp. 2574–2589, 2017.
- [29] T. Lu, Q. Liu, X. He, H. Luo, E. Suchyta, J. Choi, N. Podhorszki, S. Klasky, M. Wolf, T. Liu, and Z. Qiao, "Understanding and modeling lossy compression schemes on HPC scientific data," in *2018 IEEE International Parallel and Distributed Processing Symposium (IPDPS)*, May 2018, pp. 348–357.
- [30] D. Tao, S. Di, X. Liang, Z. Chen, and F. Cappello, "Optimizing lossy compression rate-distortion from automatic online selection between sz and zfp," *IEEE Transactions on Parallel and Distributed Systems*, vol. 30, no. 8, pp. 1857–1871, 2019.